Athermal Crystal Defects Dynamics in Si Revealed by Cryo-High-Voltage Electron Microscopy

Kazuhisa Sato[*, †, ‡] and Hidehiro Yasuda[†, ‡]

[†]Research Center for Ultra-High Voltage Electron Microscopy, Osaka University

7-1 Mihogaoka, Ibaraki, Osaka 567-0047, Japan

[‡]Division of Materials and Manufacturing Science, Graduate School of Engineering, Osaka University, 2-1 Yamadaoka, Suita, Osaka 565-0871, Japan

*E-mail address: sato@uhvem.osaka-u.ac.jp

ABSTRACT:

Low temperature crystal defects dynamics in Si has been studied by a newly developed cryo-high-voltage electron microscopy. The planar {113} defects of self-interstitial atoms were introduced at 94 K by 1 MeV electron irradiation with damage higher than 0.42 displacements per atom (dpa), unlike past findings. The defects once grew and then shrunk during the observation. We show that the nucleation and the dissociation dynamics of the {113} defects can be attributed to an athermal process, which is deduced from anomalously fast diffusion of self-interstitial atoms at a low temperature.

KEYWORDS: *electron irradiation, silicon, self-interstitials, athermal process, cryo-high-voltage electron microscopy*

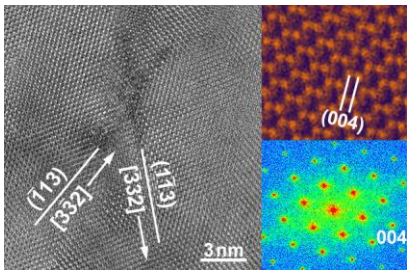

INTRODUCTION

High-voltage transmission electron microscopy (HVEM) is a powerful tool to characterize interior structures of a micrometer-thick specimen with a high spatial resolution. To date a plenty of useful findings regarding materials physics such as crystal defects, phase transition, and mechanical properties have been obtained by HVEM[1–3]. Recently, installation of a high-performance direct electron detection (DED) CMOS camera has significantly improved the performance of the HVEM. For example, structural dynamics of nanoparticles has been revealed in sub-millisecond to a millisecond time scale[4, 5], which could not be detected by a conventional CCD camera so far. As a result, in addition to the high spatial resolution and high penetration power[6, 7], the latest HVEM opens up a new horizon for *in-situ* characterization of materials' structure-property relationships. Recent developments of the HVEM are not limited to the aforementioned detection system; we have successfully installed a cryogenic specimen stage to our HVEM (cryo-HVEM). In general, cryo-EM (typically, 200-300 kV-class TEM) has been used to observe biological samples and soft materials that are sensitive to electron radiation damage[8-12]. It features an imaging system capable of observing images with a low electron dose together with a dedicated specimen stage cooled by liquid nitrogen. In our newly developed cryo-HVEM, up to 12 specimens are stored in the inner storage that is always cooled with liquid nitrogen, and a selected specimen is transferred to the observation position in the pole piece gap by the autoloader system.

Radiation damage in silicon (Si) induced by MeV electron irradiation has been studied for over 40 years. The main conclusion is that in most cases point defects and their assemblies such as {113} defects are introduced by MeV electron irradiation above room temperature, especially at 673–823 K[13–16], and amorphization can only be realized under limited conditions

at low temperatures with a high electron dose[17, 18]. Here we report on the structural properties of a Si single crystal at a low temperature obtained using the novel cryo-HVEM. Mechanical stability of our new cryo-HVEM makes the atomic resolution observation possible at liquid nitrogen temperature. By low dose observation using a DED camera, we observed formation of planar {113} defects of self-interstitials even at a low temperature.

RESULTS

Figure 1a shows a high-resolution TEM (HREM) image of Si obtained at 94 K with beam incidence in the $[110]_{Si}$. The observation was performed at an area about 500 nm from the specimen edge ("edge" means the boundary between the specimen and a hole opened by the Ar ion milling). As seen, Si(110) dumbbells, 136 pm in distance, are observed as lattice images. Corresponding Fast Fourier transform (FFT) pattern is shown in Figure 1b. The unusual diffuse contrast from the top left to the bottom right of the image is due to drift correction (< 100 pm) and image integration. It is worth noting that 008 reflection seen in the FFT pattern which corresponds to 67 pm in real space indicates the mechanical stability of the cryo-stage kept at 94 K. Also $\bar{4}40$ reflection (96 pm) is seen in the orthogonal direction. Figure 1c shows a selected area electron diffraction (SAED) pattern obtained from an area ~600 nm in diameter. Note that the pattern is free from a halo ring of amorphous SiO_2: a surface damaged layer by Ar ion milling is presumed to be extremely thin.

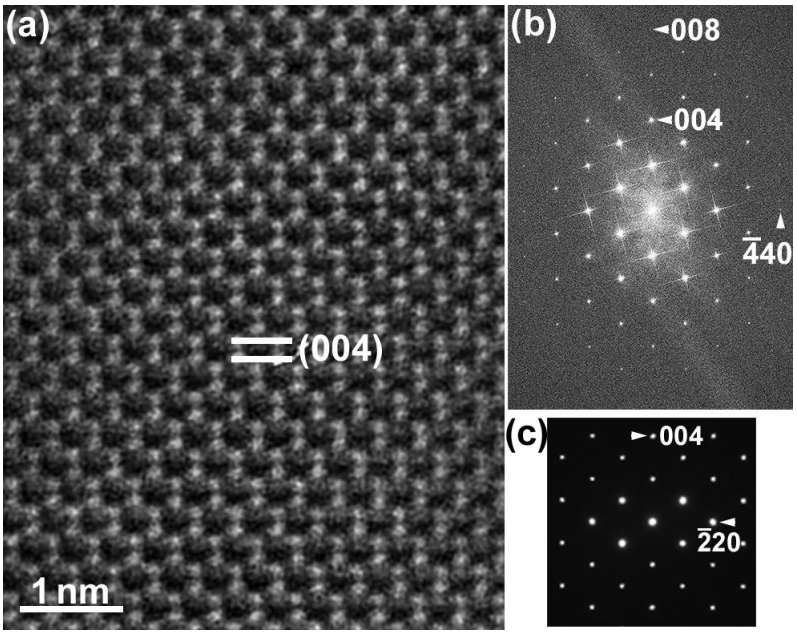

Figure 1. (a) Lattice image of Si obtained at 94 K. The beam incidence is in the $[110]_{Si}$. (b) FFT pattern processed from the image shown in (a). (c) SAED pattern obtained with the beam incidence of $[110]_{Si}$.

Figure 2 shows a representative HREM image of Si including lattice defects observed with beam incidence in the $[110]_{Si}$. Corresponding FFT pattern is shown in the inset. During the observation with a dose rate of 12.4 e/pixel s (=550 e/Å^{2}s) for a couple of minutes, such defects contrast suddenly appeared. It was found that the defect is the planar {113} defects of self-interstitials elongated in the <332> direction. The {113} defect was firstly found in electron-irradiated Ge[19], and then the atomic structure of the defect formed in Si was revealed in detail by TEM[16, 20, 21]. The appearance of the {113} defects in Si at 94 K is curious since this type of defects are known to appear by MeV electron irradiation at temperatures above room temperature[13–16].

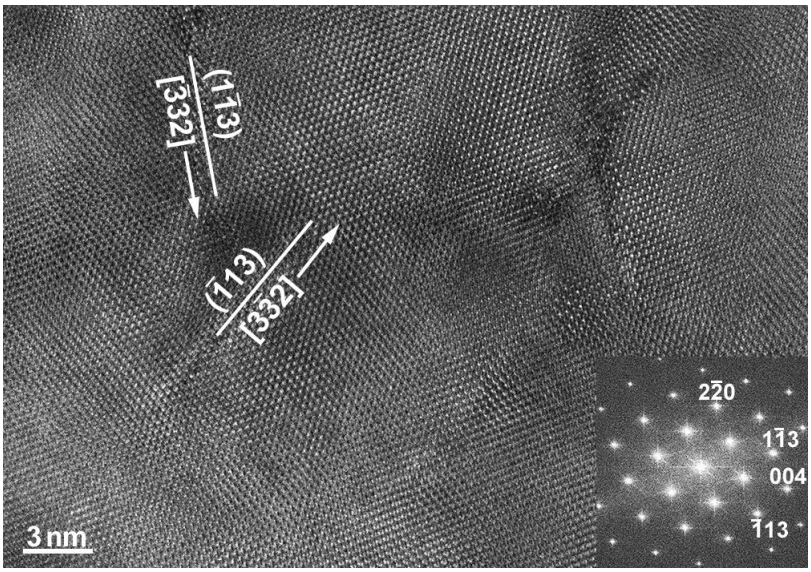

Figure 2. HREM image of Si including the planar {113} defects of self-interstitials observed at 94 K with beam incidence in the $[110]_{Si}$. Corresponding FFT pattern is shown in the inset.

Figure 3 shows a series of HREM images obtained *in-situ* with a dose rate of 18 e/pixel s (=800 e/Å^{2}s). The observation was performed at a thick area about 5 μm from the specimen edge. Thickness of the observed area is presumed to be at most 700 nm (this was estimated by our preliminary work using electron energy-loss spectroscopy). In Figure 3a (2 min after the start of observation), there is no defect contrast in the observed area. After 13 min observation (received damage of 0.42 displacements per atom (dpa)), a fine defect ~3 nm in length appeared as shown in the circle (Figure 3b). It grew as the irradiation proceeds and reached 6 nm in length after 15 min irradiation (Figure 3c, 0.48 dpa) and kept its size until 21 min irradiation (Figure 3d, 0.67 dpa). After 23 min irradiation (Figure 3e, 0.74 dpa), the defect shrunk and a new defect as shown by an arrow appeared alternatively in the immediate vicinity. The appearance of new defects in a short time (< 2 min) indicates that the clustering of self-interstitials of Si is a very fast event even at 94 K. Both these defects seen in Figure 3e were

maintained after 27 min irradiation (0.87 dpa, not shown), while they disappeared after 35 min irradiation (Figure 3f, 1.14 dpa).

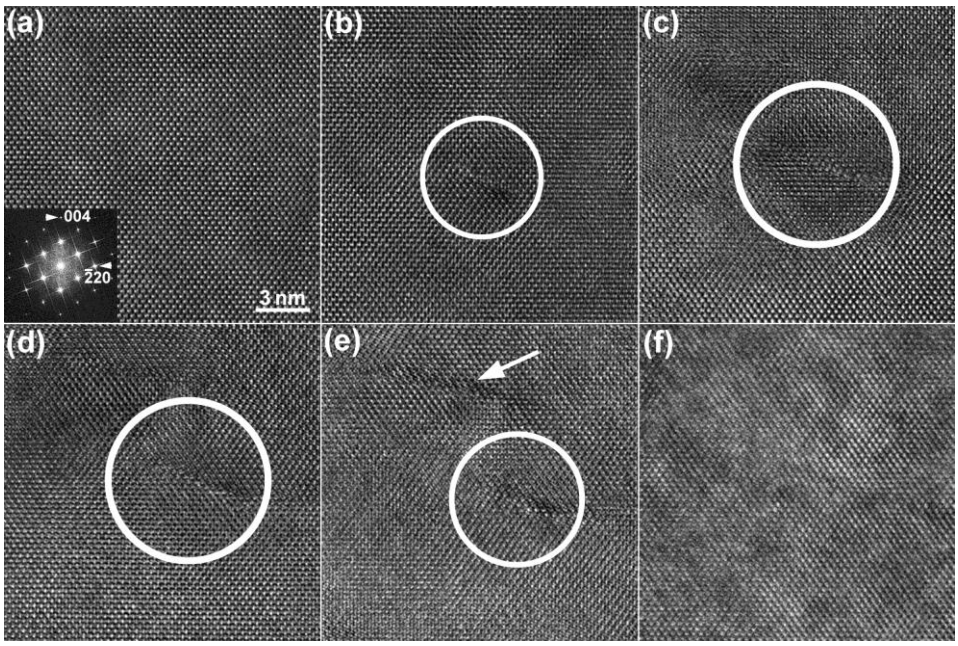

Figure 3. Series of HREM images obtained in-situ with a dose rate of 18 e/pixel s (=800 e/Å^{2}s = 8.0×10^{22} e/m^{2}s) at 94 K. (a) 9.6×10^{24} e/m^2 (0.06 dpa), (b) 6.2×10^{25} e/m^2 (0.42 dpa), (c) 7.2×10^{25} e/m^2 (0.48 dpa), (d) 1.0×10^{26} e/m^2 (0.67 dpa), (e) 1.1×10^{26} e/m^2 (0.74 dpa), (f) 1.7×10^{26} e/m^2 (1.14 dpa).

We also investigated defects motion under prolonged irradiation at 94 K. After obtaining the image shown in Figure 3f (35 min irradiation, 1.14 dpa), we found formation of another defect in the field of view. Figure 4a shows an HREM image of the above newly formed {113} defect observed after 40 min irradiation (5 min irradiation after the formation, total damage: 1.27 dpa). As seen, the defect gradually shrunk with irradiation (Figures 4b–d), while it once regrown after 60 min irradiation (Figure 4e, 1.95 dpa), and it shrunk again after 67 min (Figure

4f, 2.15 dpa). As shown in Figures 3 and 4, it was found that the {113} defects were generated and then disappeared at about 30 min intervals during the 1 MeV electron irradiation at 94 K. These results imply that dynamics of the planar {113} defects of self-interstitials can be attributed to an athermal process.

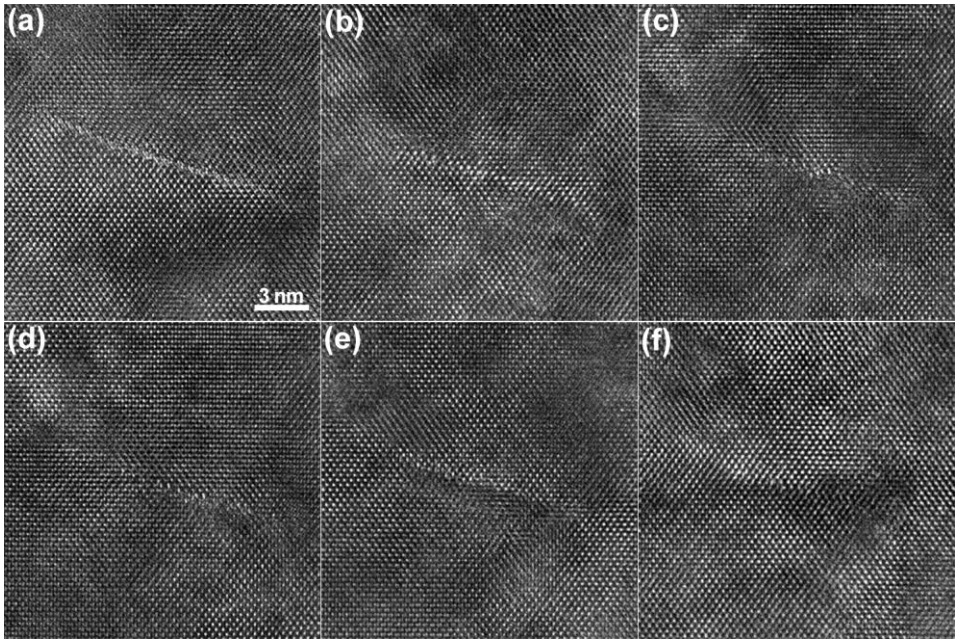

Figure 4. Series of HREM images obtained in-situ with a dose rate of 18 e/pixel s (=800 e/Å^{2}s = 8.0×10^{22} e/m^{2}s) at 94 K. (a) 1.9×10^{26} e/m^2 (1.27 dpa), (b) 2.5×10^{26} e/m^2 (1.68 dpa), (c) 2.6×10^{26} e/m^2 (1.74 dpa), (d) 2.7×10^{26} e/m^2 (1.81 dpa), (e) 2.9×10^{26} e/m^2 (1.95 dpa), (f) 3.2×10^{26} e/m^2 (2.15 dpa).

Figures 5a and 5b show irradiation time dependence of the length of {113} defects in the <332> direction extracted from the results obtained in Figures 3 and 4, respectively. Although the defocus was fine-tuned so that sharp defects contrast can be obtained, the measured length is the apparent value since size and shape of a planar {113} defect in the [110] direction

(electron propagation direction) are unknown. The error bars were estimated from the spread of the defect contrast in the direction perpendicular to the defect plane. As seen, defects are formed and grown, and after maintaining a certain size for a while, they tend to disappear by further irradiation. We deduced the diffusivity of self-interstitials to be 3.8–7.5 × 10^{-20} m^2s^{-1} for growth and 4.3–6.4 × 10^{-20} m^2s^{-1} for shrunk. According to the literature[22], the obtained diffusivity corresponds to a value expected for self-diffusion of self-interstitials at 1250 K (a frequency factor of 0.53 m^2s^{-1} and an activation energy of 4.75 eV were used for estimation). Thus, diffusion of self-interstitials is significantly enhanced under 1 MeV electron irradiation at 94 K. This result indicates that the defects motion is not a thermally activated process under the present experimental conditions.

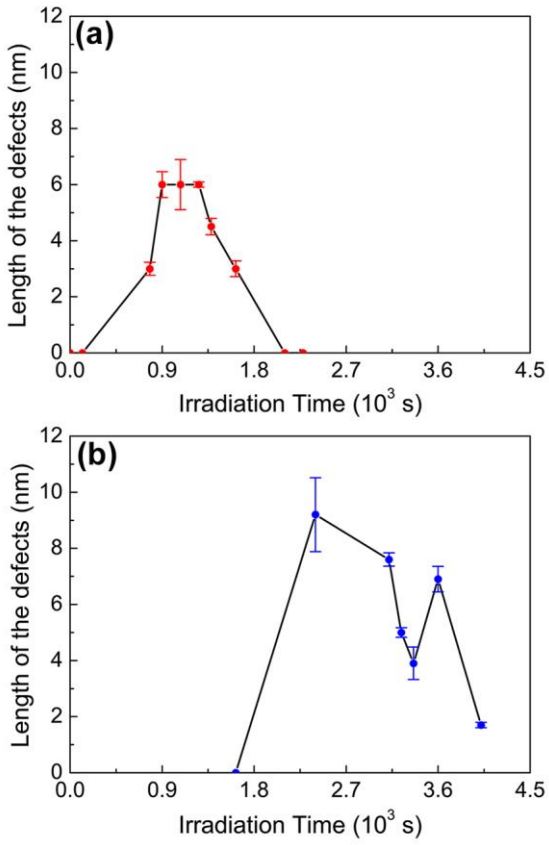

Figure 5. Irradiation time dependence of the length of {113} defects in the <332> direction. (a) and (b) are extracted from the results obtained in Figures 3 and 4, respectively.

DISCUSSION

Formation of {113} defects by MeV electron irradiation has been extensively studied in the temperature range above room temperature, especially at 673-823 K[13, 14, 16]. Vanhellemont et al. reported that rate of the {113} defects formation under 2 MeV electron irradiation is reduced at room temperature compared to that of at 573 K[23]. Also note that the {113} defects are formed at relatively high temperatures, while voids are introduced at lower temperatures as reported in the literature[24]. The experimentally determined border of the formation temperature between {113} defects and voids is in the temperature range between 100 K and 200 K[24]. In this study, we found that the {113} defects are also introduced by 1 MeV electron irradiation at 94 K. The irradiation temperature of 94 K is just below the lower limit of the aforementioned border. Electron dose required for the defect formation was in the order of 10^{25} e/m^2, which is comparable to those reported on most of the previous studies (10^{25}–10^{26} e/m^2). It has been reported that increasing the oxygen content in Si reduces the formation rate of the {113} defects[23], while that increasing the partial pressure of oxygen in the atmosphere enhances the defects formation[25]. Oxygen acts as a sink for vacancies, forming V-O pairs, which eventually leads to recombination with interstitials[23, 26]. In this study, low energy ion milling effectively reduced surface oxide and a possible damaged layer, as evidenced by the fact that obvious halo rings of amorphous SiO_2 was not observed in the SAED pattern (Figure 1c) as well as the FFT patterns of HREM images (Figure 1b, inset of Figures 2 and 3a); the specimen surface will be coated by thin native oxide. Specimen chamber of the cryo-HVEM is evacuated by turbo-molecular pumps and sputter-ion pumps, and maintains a vacuum of approximately 1×10^{-5} Pa during the observation. Furthermore, since the cryogenic specimen stage is cooled with liquid

nitrogen all the time, residual H_2O vapor will be eliminated by adsorption. Thus, electron irradiation was performed in a clean condition excluding contamination sources as much as possible.

Similar phenomena, the formation and disappearance of {113} defects, as observed in this study, were previously found by 1 MeV irradiation at room temperature[15]. The motion of the defects was reported at the electron dose of 0.6–1.3 × 10^{26} e/m^2, and these values are almost equivalent to the dose used in this study. As we have shown in the present study, the {113} defects formation, usually induced at higher temperatures, also occur at a low temperature. Such a low temperature structural dynamics indicates an athermal process as the formation mechanism of the {113} defect, and it also explains the dissociation of the defects during the 1 MeV electron irradiation at 94 K. Since the dynamics is not a thermally activated process, {113} defects are presumed to be able to grow and shrink at a very high speed as observed in this study. It should be noted that the {113} plane of the diamond structure consists of 12 equivalent planes, and when a {113} defect satisfies the edge-on condition with respect to the incident electron beam, the linear defect contrast can be clearly observed, as shown in Figures 2–4. It is presumed that the disappearance of the defects under 1 MeV electron irradiation is due to migration of interstitial atoms to an equivalent plane, which does not satisfy the edge-on condition, or annihilation at the specimen surface. Shrinkage of the defects can also be explained by the purification of the irradiated area by the absorption of pre-existing impurities into interstitial clusters[27]. Since {113} defects are not formed in a thin region near the specimen edge[16], observation in a thick region is essential for such defects dynamics characterization. The veiled phenomenon was hence detected by the experiment simultaneously satisfying the following three conditions using a sufficiently thick specimen: low temperatures (< 100 K),

high-energy electron irradiation (1 MeV), and atomic resolution. Thus we have demonstrated that the novel cryo-HVEM has a high potential in a research of irradiation-induced defects and their dynamics.

Regarding lattice defects characterization of a thick specimen, the authors recently demonstrated that bright-field scanning transmission electron microscopy (BF-STEM) mode in the HVEM shows extreme penetration power[6]. In fact, it has been demonstrated that dislocations in Si can be observed even at a thickness of 14 μm using the 1 MV-STEM[28, 29]. In this study we focused on HREM imaging using the cryo-HVEM, while in the future, STEM in cryo-HVEM has potential to reveal crystal defects in a thicker specimen that can be regarded as bulk.

CONCLUSIONS

We have studied lattice defects dynamics in Si at 94 K using a newly developed cryo-HVEM operating at 1 MV. Lattice images resolved Si(110) dumbbells of 136 pm distance and the FFT pattern of the image showed the 008 reflection corresponding to 67 pm in real space. We found that the planar {113} defects of self-interstitial atoms, usually formed at temperatures above room temperature, appear at 94 K by 1 MeV electron irradiation with damage higher than 0.42 dpa. The defects once grew and then shrunk during the observation. Diffusivity of self-interstitials at 94 K during 1 MeV electron irradiation was deduced to 10^{-20} m^2/s in order, which corresponds to a value of self-diffusion of self-interstitials at 1250 K. High-diffusivity at a low temperature indicates that the {113} defects dynamics can be attributed to an athermal process instead of a thermally activated process. We show that novel cryo-HVEM has a high potential in the research of irradiation-induced defects and their dynamics.

METHODS

TEM specimens of a Si single crystal were prepared in the following manner. First, a small piece of Si(110) wafer (Cz, p-type, 8–12 Ωcm) ca 2 × 2 × 0.5 mm^3 in size was glued on a Mo single hole grid 3 mm in diameter. Then the crystal was thinned by mechanical polishing, and finally a small hole was made at the center of the specimen by low-energy Ar ion milling. The prepared specimen was cooled using liquid nitrogen and then transferred to the specimen stage of the cryo-HVEM. We confirmed that the area of interest of the sample was not broken or damaged by immersion in liquid nitrogen. Microstructures of the specimens prepared as above and loaded on the cryogenic stage were characterized by JEOL JEM-1000EES cryo-HVEM installed in Osaka University operating at 1 MV equipped with a LaB_6 cathode. The spherical aberration coefficient (C_s) and the chromatic aberration coefficient (C_c) of the cryo-HVEM are 4.1 mm and 5.1 mm, respectively. The stage temperature was kept at 94 K during the TEM observation. Electron imaging as well as electron irradiation were performed with a beam incidence in the $[110]_{Si}$ direction. HREM images were recorded using a DED camera (Gatan K2 summit, 4k × 4k). HREM images were obtained with a dose rate of 5.5 × 10^{22} – 8.0 × 10^{22} e/m^2s (550–800 e/Å^{2}s). Note that the K2 summit camera can be operated at low electron doses and it accepts at most 20 e/pixel s (=890 e/Å^{2}s). The cross section (σ) of atomic displacements of Si was estimated to be 67.1 barns (67.1 × 10^{-28} m^2) under 1 MeV electron irradiation based on the McKinley-Feshbach formula[30] for the collision between an electron of charge e with a nucleus of charge Ze:

$$\sigma = \pi\left(\frac{Ze^2}{mc^2}\right)^2\left(\frac{1}{\beta^4\gamma^2}\right)\left[\left(\frac{T_m}{T_d}-1\right)-\beta^2 ln\frac{T_m}{T_d}+\pi\alpha\beta\left\{2\left[\left(\frac{T_m}{T_d}\right)^{\frac{1}{2}}-1\right]-ln\frac{T_m}{T_d}\right\}\right] \quad (1)$$

where Z is the atomic number, m is the rest mass of electron, c is the velocity of light, v is the

velocity of electron with $\beta = v/c$ and $\gamma = (1-\beta^2)^{-1/2}$, T_m is the maximum recoil energy, T_d is the displacement threshold energy (T_d = 13 eV [31] and T_m = 155 eV for Si under 1 MeV electron irradiation). Size of each HREM image is 3710 × 3390 pixels with a pixel size of 0.015 nm. Each image was taken at an exposure time of 0.8 s, and a total of 10 images were integrated with drift correction. SAED patterns were recorded using a charge-coupled device (CCD) camera (Gatan Orius SC200, 2k × 2k).

ACKNOWLEDGMENTS

The authors wish to thank Mr. A. Ohsaki, Mr. S. Takakuwa, and all the members of JEOL Ltd. involved in construction of the JEM-1000EES cryo-HVEM. KS acknowledges Dr. J. Yamasaki of Osaka University for invaluable comments. This study was partially supported by the JSPS KAKENHI Grant Number JP17H02746.

AUTHOR INFORMATION

*Email addresses:

sato@uhvem.osaka-u.ac.jp (K. Sato) (corresponding author)

yasuda@uhvem.osaka-u.ac.jp (H. Yasuda)

ORCID

Kazuhisa Sato: 0000-0001-9078-2541

Hidehiro Yasuda: 0000-0002-9877-9803

Author Contributions

All authors contributed to the discussion and writing of the manuscript. The final version of the manuscript was approved by all authors.

Notes

The authors declare no competing financial interest.

REFERENCES

(1) Fujita, H. Ultra-high voltage electron microscopy: past, present, and future. *J. Electron Microsc. Tech.* **1986**, *3*, 243–304.

(2) Seeger, A. Four generations of high-voltage electron microscopes. *J. Electron Microsc.* **1998**, *4*, 301–315.

(3) Mori, H. Topics in recent studies of high-voltage electron microscopes. *J. Electron Microsc.* **2011**, *60*, S189–S197.

(4) Yasuda, H. Fast in situ ultrahigh-voltage electron microscopy observation of crystal nucleation and growth in amorphous antimony nanoparticles. *Cryst. Growth and Design* **2018**, *18*, 3302–3306.

(5) Sato, K.; Yasuda, H. Fluctuation of long-range order in Co-Pt alloy nanoparticles revealed by time-resolved electron microscopy. *Appl. Phys. Lett.* **2017**, *110*, 153101.

(6) Sato, K.; Yasuda, H. Probing crystal dislocations in a micrometer-thick GaN film by modern high-voltage electron microscopy. *ACS Omega* **2018**, *3*, 13524–13529.

(7) Yamasaki, J.; Ubata, Y.; Yasuda, H. Empirical determination of transmission attenuation curves in mass-thickness contrast TEM imaging. *Ultramicrosc.* **2019**, *200*, 20–27.

(8) Fujiyoshi, Y.; Mizusaki, T.; Morikawa, T.; Yamagishi, H.; Aoki, Y.; Kihara, H.; Harada, Y. Development of a superfluid helium stage for high-resolution electron microscopy. *Ultramicrosc.* **1991**, *38*, 241–251.

(9) Frank J. *Three-dimensional electron microscopy of macromolecular assemblies*, Oxford University Press: Oxford, 2006.

(10) Vinothkumar, K. R.; Henderson, R. Single particle electron cryomicroscopy: trends, issues and future perspective. *Quarterly Reviews of Biophysics* **2016** *49* e13 1–25.

(11) Masuda, H.; Yasuda, H.; Onoe, J. Two-dimensional periodic arrangement of one-dimensional polymerized C_{60} evidenced by high-resolution cryo-transmission electron microscopy. *Carbon* **2016**, *96*, 316–319.

(12) Nakanishi, A.; Kishikawa, J.; Tamakoshi, M.; Mitsuoka, K.; Yokoyama, K. Cryo EM structure of intact rotary H^+-ATPase/synthase from Thermus thermophiles. *Nature Comm.* **2018**, *9*, 89.

(13) Matthews, M. D.; Ashby, S. J. The dynamic observation of the formation of defects in silicon under electron and proton irradiation. *Phil. Mag.* **1973**, *27*, 1313–1322.

(14) Salisbury, I. G.; Loretto, M. H. {113} loops in electron-irradiated silicon. *Phil. Mag. A* **1973**, *39*, 317–323.

(15) Hirabayashi, M.; Hiraga, K.; Shindo, D. High resolution imaging by 1 MV electron microscopy. *Ultramicrosc.* **1982**, *9*, 197–202.

(16) Takeda, S.; Muto, S.; Hirata, M. Transmission electron diffraction pattern of electron-irradiation-induced {113}-faulted loops in Si. *Jpn. J. Appl. Phys.* **1990**, *29*, L1698–L1701.

(17) Takeda, S.; Yamasaki, J. Amorphization in Si by electron irradiation. *Phys. Rev. Lett.* **1999**, *83*, 320–323.

(18) Yamasaki, J.; Takeda, S. Elemental process of amorphization induced by electron irradiation in Si. *Phys. Rev. B* **2002**, *65*, 115213.

(19) Ferreira Lima, C. A.; Howie, A. Defects in electron-irradiated germanium. *Philos. Mag.* **1976**, *34*, 1057–1071.

(20) Takeda, S. An atomic model of electron-irradiation-induced defects on {113} in Si. *Jpn. J. Appl. Phys.* **1990**, *30*, L639–L642.

(21) Takeda, S.; Kohyama, M.; Ibe, K. Interstitial defects on {113} in Si and Ge Line defect

configuration incorporated with a self-interstitial atom chain. Phil. Mag. A **1994**, *70*, 287–312.

(22) Bracht, H.; Haller, E. E.; Clark-Phelps, R. Silicon self-diffusion in isotope heterostructures. *Phys. Rev. Lett.* **1998**, *81*, 393–396.

(23) Vanhellemont, J.; Yasuda, H.; Tokumoto, Y.; Ohno, Y.; Suezawa, M.; Yonenaga, I. 2 MeV e-irradiation UHVEM study on the impact of O and Ge doping on {113}-defect formation in Si. *Phys. Status Solidi. A* **2012**, *209*, 1902–1907.

(24) Yamasaki, J.; Ohno, Y.; Takeda, S.; Kimura, Y. Phil. Mag. **2003**, 83, 151–163 (2003).

(25) Koto, K.; Takeda, S.; Ichihashi, T.; Iijima, S. Effects of O_2 on the {113} defect formation in Si observed by in situ ultrahigh vacuum transmission electron microscopy. *Appl. Phys. Lett.* **1997**, *71*, 1661–1663.

(26) Hayes, W.; Stoneham, A. M. *Defects and Defect Processes in Nonmetallic Solids*, Dover: NY, 1985.

(27) Nakai, K.; Hamada, K.; Satoh, Y.; Yoshiie, T. Effect of impurities on the growth of {113} interstitial clusters in silicon under electron irradiation. *Philos. Mag.* **2011**, *91*, 421–436.

(28) Sato, K.; Yamashita, Y.; Yasuda, H.; Mori, H. Maximum usable thickness revisited: imaging crystal dislocations in Si by modern high-voltage scanning transmission electron microscopy. *Jpn. J. Appl. Phys.* **2017**, *56*, 100304.

(29) Sato, K.; Yamashita, Y.; Yasuda, H.; Mori, H. High-voltage scanning transmission electron microscopy: a tool for structural characterization of micrometer-thick specimens. *Mater. Trans.* **2019**, *60*, 675–677.

(30) Corbett, J. W. *Electron Radiation Damage in Semiconductors and Metals*, Academic Press, NY, 1966.

(31) Urban, K. Radiation-induced processes in experiments carried out in-situ in the high-voltage electron microscope. *Phys. Stat. Sol. (a)* **1979**, *56*, 157–168.